



A New Methodology for Upscaling Semi-submersible Platforms for Floating Offshore Wind Turbines

Kaylie L. Roach¹, Matthew A. Lackner¹, James F. Manwell¹

¹Mechanical Engineering, University of Massachusetts Amherst, Amherst, MA, 01003, USA

5 *Correspondence to:* Matthew A. Lackner (lackner@ecs.umass.edu)

Abstract. This paper presents a new upscaling methodology for floating offshore wind turbine platforms. The size and power rating of offshore wind turbines have been growing in recent years, with modern wind turbines rated at 10 - 14 MW in contrast with 2 - 5 MW in 2010. It is not apparent how much further wind turbines can be increased before it is unjustified. Scaling relations are a useful method for analyzing wind turbine designs, to understand the mass, load, and cost increases with size.

10 Scaling relations currently do not exist but are needed for floating offshore platforms to understand how the technical and economic development of floating offshore wind energy may develop with increasing turbine size. In this paper, a hydrodynamic model has been developed to capture the key platform response in pitch. The hydrodynamic model is validated using OpenFAST, a high-fidelity offshore wind turbine simulation software. An upscaling methodology is then applied to two semi-submersible case studies, in which the platform pitch angle at rated wind turbine thrust is constrained to a specified value.

15 The results show that platform dimensions scale to a factor of 0.75, and the platform steel mass scales to a factor of 1.5 when the wall thickness is kept constant. This study is the first to develop generalized upscaling relations that can be used for other semi-submersible platforms, in contrast with other studies that upscale a specific design to a larger power rating. This upscaling methodology provides new insight into trends for semi-submersible platform upscaling as turbine size increases.

1 Introduction

20 Offshore wind energy development continues to accelerate, and until now most offshore wind installations have used fixed-bottom support structures (Musial *et al.*, 2022). Offshore wind turbines are now planned for areas with deeper water depths including the coastlines of California (Speer, Keyser and Tegen, 2016; Beiter *et al.*, 2020), Japan (Yoshimoto *et al.*, 2013), and Europe (Ågotnes *et al.*, 2013), where floating offshore wind turbines (FOWTs) are needed (Jonkman, J. M., Matha, 2011; Musial *et al.*, 2016). Floating platforms have been designed and deployed in pilot projects such as the Fukushima FORWARD

25 project in Japan (Fukushima Offshore Wind Consortium, no date; Karimirad, 2014; Kikuchi and Ishihara, 2019a), the Hywind project in Scotland (Skaare *et al.*, 2006; Karimirad, 2014; Equinor, 2021), and the WindFloat deployments in Portugal (Principle Power, no date; Karimirad, 2014; Beaubouef, 2020) and Scotland (Durakovic, 2021) with turbine power ratings of 2 MW - 9.5 MW, while others are planned for the U.S. in California (California Energy Commission, 2021; Conversation, 2021) and Maine (The University of Maine, 2021).



30 Offshore wind turbine size and capacity have been growing rapidly over the past ten years as well. Modern offshore wind turbines designed by General Electric, Siemens Gamesa, and Vestas have ratings of 10 - 15 MW with blade diameters exceeding 200 m (Siemens Gamesa, 2020; GE Renewable Energy, 2023; Vestas, 2023). In contrast, in 2010 offshore turbines had power ratings between 2 - 5 MW and blade diameters were 75 - 125 m (Musial *et al.*, 2022). Even larger designs are likely to be developed in the future, with researchers even investigating a 50 MW offshore turbine (Yao *et al.*, 2021).

35 While the industry is clearly trending towards larger wind turbines, the classical “cubed-square” law dictates that the per MW capital cost of a wind turbine increases with turbine size due to the mass increasing more quickly than the rated power (Manwell, McGowan and Rogers, 2009). However, looking at data of historic wind turbines, the cost does not scale with the mass because of technological innovations over time. Also, the industry trend towards larger offshore wind turbines minimizes the number of installed units in a wind farm for a given total capacity, which is motivated by the large per unit cost (including
40 the foundation, installation, electrical interconnection, and maintenance visits at sea). Offshore wind levelized cost of energy (LCOE) is still about twice as much as onshore wind on average, but as turbine size has increased, LCOE has decreased significantly over time (Thresher, Robinson and Veers, 2008; Beiter *et al.*, 2016). As offshore wind energy development continues, it is important to understand if even larger turbines can continue to reduce the LCOE of offshore wind farms, or if there is an upper limit to the cost effectiveness and practicality of upscaling.

45 The process of evaluating a wind turbine design with increasing scale is referred to as “upscaling.” Classical upscaling methods can be used to project the power, size, mass, forces, moments, costs, and other properties of an upscaled turbine based on a turbine of a smaller size (Manwell, McGowan and Rogers, 2009). Upscaling methods are discussed further in Section 2. As wind turbines are rapidly increasing in power rating, research is needed to understand how the design characteristics of FOWT platforms, including the physical dimensions, mass, cost, and dynamic behavior, change with respect to the increased turbine
50 size.

This paper aims to model and analyze semi-submersible FOWT platform design characteristics and system dynamics to provide insight into technology development of FOWT systems with larger power ratings. The objective is to develop general scaling trends, which characterize the mass, dimensions, and dynamics of the semi-submersible FOWT platform subject to constraints on the system stability as a turbine is upscaled. To achieve this objective, a new upscaling methodology for floating
55 platforms is developed based on a hydrodynamic model that captures the key platform responses in pitch. The hydrodynamic model is validated using OpenFAST, a high-fidelity offshore wind turbine simulation software (Jonkman, 2019; National Renewable Energy Laboratory, 2020). The methodology is then applied using two semi-submersible case studies, in which the platform pitch angle at rated wind turbine thrust is constrained to a constant value. Other researchers have upscaled specific semi-submersible platforms (George, 2014; Leimeister *et al.*, 2016; Ju *et al.*, 2020; Kikuchi and Ishihara, 2020). This study is
60 the first to develop generalized upscaling relations for semi-submersible FOWT platforms, and provides new insight into design trends as turbine size increases. Additionally, the paper identifies key underlying physics behind the semi-submersible upscaling relations.



This paper is organized as follows: Section 2 provides a review of literature. Section 3 describes the methods used in this research study, including the hydrodynamic modeling of floating offshore platforms, the semi-submersible case studies, the model validation, and upscaling methodology. Section 4 presents the upscaling results, as well as a new analytical model for FOWT upscaling and parameter sensitivity studies. Finally, Section 5 summarizes the research findings and future work.

2 Background

Classical upscaling relations have been developed for a wind turbine with geometric and aerodynamic similarity (Manwell, McGowan and Rogers, 2009; Ashuri, 2012; Sieros *et al.*, 2012). The general form of the scaling relations is shown in Eq. (1). The upscaled parameter (denoted with subscript 2) depends on the ratio of the upscaled to the original rotor radius (R), original parameter size (denoted with subscript 1), and the scale dependence power α . Table 1 shows the scaling relations for power, forces, weight, moments, stresses, and resonances for a wind turbine (Manwell, McGowan and Rogers, 2009).

$$\frac{\text{Parameter}_1}{\text{Parameter}_2} = \left(\frac{\text{Radius}_1}{\text{Radius}_2}\right)^\alpha = R^\alpha \quad (1)$$

Table 1: Classical Scaling Relations (Manwell, McGowan and Rogers, 2009)

Quantity	Symbol	Relation	Scale dependence
Power, forces, and moments			
Power	P	$P_1/P_2 = (R_1/R_2)^2$	$\sim R^2$
Torque	Q	$Q_1/Q_2 = (R_1/R_2)^3$	$\sim R^3$
Thrust	T	$T_1/T_2 = (R_1/R_2)^2$	$\sim R^2$
Rotational speed	Ω	$\Omega_1/\Omega_2 = (R_1/R_2)^1$	$\sim R^{-1}$
Weight	W	$W_1/W_2 = (R_1/R_2)^3$	$\sim R^3$
Aerodynamic moments	M_A	$M_{A,1}/M_{A,2} = (R_1/R_2)^3$	$\sim R^3$
Centrifugal forces	F_c	$F_{c,1}/F_{c,2} = (R_1/R_2)^2$	$\sim R^2$
Stresses			
Gravitational	σ_g	$\sigma_{g,1}/\sigma_{g,2} = (R_1/R_2)^1$	$\sim R^1$
Aerodynamic	σ_A	$\sigma_{A,1}/\sigma_{A,2} = (R_1/R_2)^0 = 1$	$\sim R^0$
Centrifugal	σ_c	$\sigma_{c,1}/\sigma_{c,2} = (R_1/R_2)^0 = 1$	$\sim R^0$
Resonances			
Natural frequency	ω	$\omega_{n,1}/\omega_{n,2} = (R_1/R_2)^1$	$\sim R^{-1}$
Excitation	Ω/ω	$(\Omega_1/\omega_{n,1})/(\Omega_2/\omega_{n,2}) = (R_1/R_2)^0 = 1$	$\sim R^0$
Note: R , radius			

The rotor power is related to the scaling factor squared (R^2), because it is proportional to rotor swept area. The weight of the wind turbine rotor increases with R^3 because of the volumetric upscaling with geometric similarity (Manwell, McGowan and Rogers, 2009). This “square-cube law” therefore implies that mass will increase more quickly than rated power as a turbine is upscaled, which would seem to argue against increasing the turbine size. The aerodynamic stresses are independent of rotor size, while stresses due to the blade weight increase in proportion to the rotor radius and may eventually drive the design loads for an upscaled rotor.



Historical data from wind turbines of different sizes can also be used to understand upscaling trends. For example, historical data indicates that the rotor mass has increased to the power of between 2 and 2.5, not the cubic power of the square-cube law (Figure 1) (Jamieson, 2018). This smaller value for the scaling exponent is primarily due to technological innovation, such as new materials and improved manufacturing, in newer designs that are usually larger in size (Jamieson, 2018; Shields *et al.*, 2021).

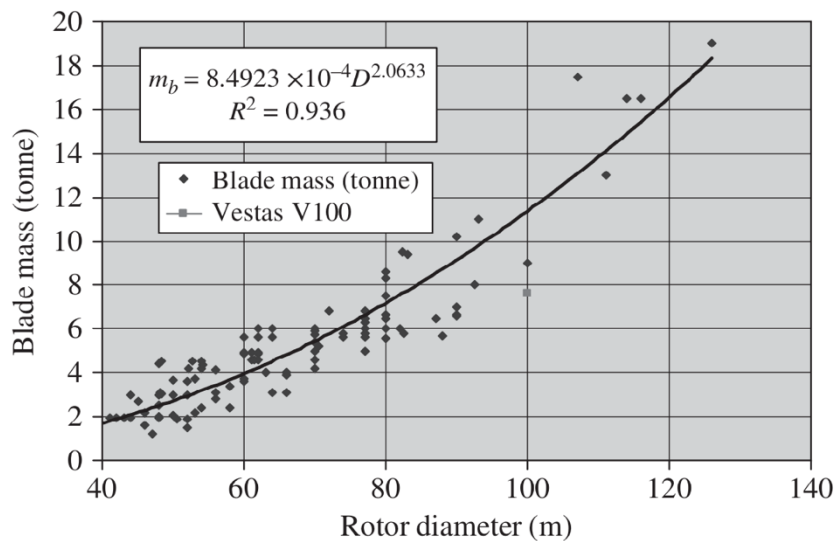


Figure 1: Blade Mass Scaling Based on Data (Jamieson, 2018)

As wind turbines become larger, the mass and aerodynamic forces increase as well, and so the floating platform that supports the turbine must grow to ensure a stable system. Several researchers have studied floating platform upscaling for a specific case study (George, 2014; Leimeister *et al.*, 2016; Ju *et al.*, 2020; Kikuchi and Ishihara, 2020), including multiple studies of semi-submersible FOWT platforms (George, 2014; Leimeister *et al.*, 2016; Kikuchi and Ishihara, 2019a). George (George, 2014) upscales the 5 MW OC4 semi-submersible FOWT to 7.5 MW and 10 MW (Robertson, A., Jonkman, J., Masciola, M., Song, 2014). Leimeister *et al.* (Leimeister *et al.*, 2016) also upscale the 5 MW OC4 reference FOWT platform to 7.5 MW. Kikuchi and Ishihara (Kikuchi and Ishihara, 2019a) upscale the 2 MW Fukushima Forward semi-submersible FOWT to 5 MW and 10 MW (Fukushima Offshore Wind Consortium, no date). Leimeister *et al.* (Leimeister *et al.*, 2016) upscale all platform parameters, and then check the static pitch of the turbine at rated wind speed to iteratively adjust parameters as needed. Both George (George, 2014) and Kikuchi and Ishihara (Kikuchi and Ishihara, 2019b) keep the draft constant due to constraints of harbor depth. The other parameters are scaled, and the static pitch is evaluated; the design is iterated until the static pitch matches the original design. Each of these three studies finds that it is technically and economically feasible to upscale the semi-submersible system. Leimeister *et al.* (Leimeister *et al.*, 2016) find that the upscaled system had to also be designed for the heave natural period, and recommends having different scaling factors for different parts of the platform.



105 Wu and Kim (Wu and Kim, 2021) have developed a methodology for upscaling a FOWT turbine and semi-submersible platform by using the 5 MW OC4 and 15 MW IEA semi-submersible systems. The central column diameter is set to be equal to the tower diameter and a guess is made for the scale factor, which is applied to the column radius and distance between columns. The buoyancy is calculated, and the ballast mass is set to match the total weight with the buoyancy. The scaling factor for the distance between columns and column radius is adjusted iteratively until the desired platform pitch angle is reached. Additionally, the same methodology is followed while keeping the column radius constant and only increasing the distance between the columns.

110 When upscaling a FOWT, specific load cases are typically used to constrain the design and ensure acceptable stability and dynamics. Load cases at rated wind speed often govern the extreme loads of FOWT systems (George, 2014; Leimeister *et al.*, 2016; Kikuchi and Ishihara, 2019a; Wu and Kim, 2021; Souza and Bachynski-Polić, 2022). Silva de Souza and Bachynski-Polic (Souza and Bachynski-Polić, 2022) study the behavior of a large spar FOWT and find that the extreme loads are governed by the rated wind speed cases rather than the extreme wind and sea state cases.

115 **3 Methodology**

In this section, a hydrodynamic model for FOWT platforms is presented, which can be used to assess the static stability and natural period of a platform based on the geometry. The hydrodynamic model is validated using OpenFAST. This model is then used in two upscaling case studies, which are carried out for two semi-submersible platforms.

3.1 Hydrodynamic Modeling of Floating Platforms

120 FOWT platforms stabilize the offshore wind turbine system, allowing the turbine to produce power while floating in the water. Figure 2 shows the three primary FOWT platform types: spar, semi-submersible, and tension leg platform (Speer, Keyser and Tegen, 2016). Floating platforms can be stabilized by ballast, buoyancy, moorings, or a combination (Wang *et al.*, 2010; Karimirad, 2014; Thiagarajan and Dagher, 2014; Speer, Keyser and Tegen, 2016). This study focuses on semi-submersible FOWT platforms, which is primarily stabilized by the large waterplane area of the offset columns, with a wider spread adding
125 more stability.

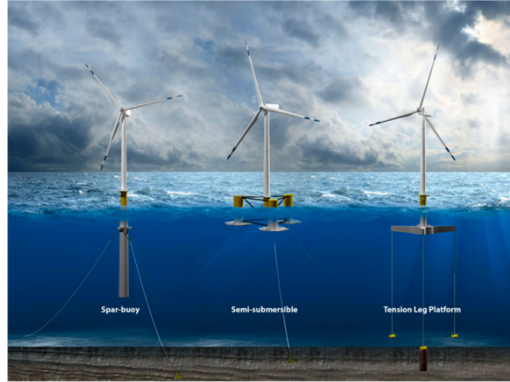


Figure 2: Types of Floating Offshore Wind Platforms (illustration by Joshua Bauer, NREL) (Speer, Keyser and Tegen, 2016)

OpenFAST is a simulation tool developed by the National Renewable Energy Laboratory used to evaluate offshore wind turbines (Jonkman, 2019; National Renewable Energy Laboratory, 2020). The aerodynamics, hydrodynamics, elastodynamics, and system controls are all incorporated into a coupled simulation. OpenFAST is widely used in academia and industry for wind turbine modeling and simulation.

The stability of a FOWT can be characterized using the hydrodynamic loading and response. Eq. (2), known as the Cummins equation, is the equation of motion for an offshore platform in water with six degrees of freedom (TU Delft, 2006; Jonkman, 2007; Duarte, Sarmiento and Jonkman, 2014). M_{ii} is the mass or mass moment of inertia term, A_{ii} is the added mass coefficient term, K_{ii} is the retardation matrix, and C_{ii} is the stiffness matrix. The platform acceleration, velocity, and displacements are represented by \ddot{q}^{tot} , \dot{q}^{tot} , and q^{tot} respectively, F_i^{waves} is the external wave loading, F_i^{rotor} is the force of the wind turbine acting on the floating platform, and h_i is the moment arm of F_i^{rotor} for rotational platform degrees of freedom. The six degrees of freedom are labeled with $i = 1, 2, \dots, 6$ and correspond to (surge, sway, heave, roll, pitch, yaw). Figure 3 shows the FOWT coordinate system (Sebastian and Lackner, 2012).

$$(M_{ii} + A_{ii})\ddot{q}^{tot} + \int_0^T K_{ii}(t - \tau)\dot{q}^{tot}(\tau)d\tau + C_{ii}q^{tot} = F_i^{waves} + F_i^{rotor} * h_i \quad (2)$$

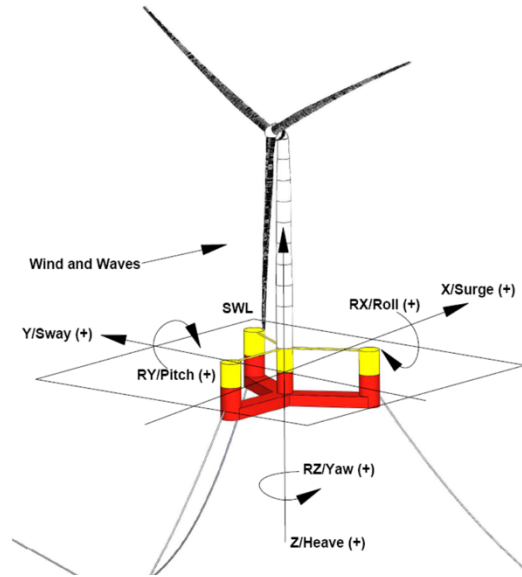


Figure 3: FOWT Platform Degrees of Freedom on IEA 15 MW System (Allen *et al.*, 2020)

When the platform is in static equilibrium, the acceleration and velocity terms are zero; ignoring the wave forcing leaves only the hydrostatic stiffness term balancing the aerodynamic forces and moments $C_{ii}q^{tot} = F_i^{rotor} * h_i$. The stiffness term, C_{ii} is
 145 comprised of both platform stiffness, $C_{ii}^{hydrostatics}$, and mooring line stiffness, C_{ii}^{lines} . This study focuses on the stiffness contributions from the platform rather than the mooring lines. The mooring lines provide a restoring force in the surge (1,1), sway (2,2), and yaw (6,6) degrees of freedom, but this study focuses primarily on the pitch (5,5) degree of freedom (Delhommeau, 1993). For the pitch degree of freedom, h_i is the distance from the system center of mass to the rotor hub.

In OpenFAST, the hydrostatic stiffness matrix, $C_{ii}^{hydrostatics}$, is defined using only the waterplane area and center of buoyancy;
 150 the center of mass is calculated separately (Jonkman, 2007). However, the hydrostatic stiffness of a platform has contributions from both gravity and buoyancy in this study, which is traditional in the field of naval architecture, and is used in the pitch angle Eq. (4) below. Eq. (3) shows the hydrostatic stiffness matrix, $C_{ii}^{hydrostatics}$, for an offshore platform (Delhommeau, 1993). The displaced volume is V_{disp} , the center of buoyancy is B , and the center of mass is CM . The matrix is symmetric, and has nonzero components including (3,3), (4,4), (5,5), (3,4), (3,5), and (4,5), corresponding to the heave (3,3), roll (4,4), and
 155 pitch (5,5) degrees of freedom.

$$C_{ij}^{hydrostatic} = \begin{bmatrix} 0 & 0 & 0 & 0 & 0 & 0 \\ 0 & 0 & 0 & 0 & 0 & 0 \\ 0 & 0 & C_{33} & C_{34} & C_{35} & 0 \\ 0 & 0 & C_{43} & C_{44} & C_{45} & 0 \\ 0 & 0 & C_{53} & C_{54} & C_{55} & 0 \\ 0 & 0 & 0 & 0 & 0 & 0 \end{bmatrix} \quad (3)$$

with:



$$C_{33} = \rho g W_0$$

$$160 \quad C_{44} = \rho g \iint_{W_0} Y^2 dW + \rho g V_{\text{disp}}(B - CM)$$

$$C_{55} = \rho g \iint_{W_0} X^2 dW + \rho g V_{\text{disp}}(B - CM)$$

$$C_{34} = C_{43} = \rho g \iint_{W_0} Y dW$$

$$C_{35} = C_{53} = -\rho g \iint_{W_0} X dW$$

$$C_{45} = C_{54} = -\rho g \iint_{W_0} XY dW$$

165 The platform has a non-zero mean pitch angle during normal operation due to aerodynamic forces. The static platform pitch angle at rated thrust (maximum thrust condition) can be calculated using Eq. (4) based on the thrust at rated wind speed, F_5^{rotor} , height from rotor nacelle assembly to the waterline, h_{hub} , and pitch stiffness $C_{55}^{\text{hydrostatics}}$.

$$\theta_p = \frac{(F_5^{\text{rotor}})(h_{\text{hub}})}{C_{55}^{\text{hydrostatics}}} \quad (4)$$

170 The natural period for offshore structures with catenary moorings is typically over 100 s in surge, sway, and yaw, and over 20 s in heave, roll, and pitch (Det Norske Veritas Germanischer Lloyd, 2017). The natural period of the system is designed to be outside the dominant period range of the wave climate, so that the structure is not excited by the ocean waves. The natural period for a moored structure is approximately given by Eq. (5) (Det Norske Veritas Germanischer Lloyd, 2017; Kikuchi and Ishihara, 2020). This research includes hydrostatic stiffness, but not mooring line stiffness; a mooring line sensitivity study is presented in section 4.6.1.

$$175 \quad T_i = 2\pi \sqrt{\frac{(M_{ii} + A_{ii})}{(C_{ii}^{\text{hydrostatics}} + C_{ii}^{\text{lines}})}} \quad (5)$$

3.2 Case Study Semi-submersible Models

180 Two semi-submersible platforms are used as case studies for upscaling. Reference FOWT systems developed by both NREL and the International Energy Agency (IEA) are selected: the OC4 5 MW semi-submersible (Robertson, A., Jonkman, J., Masciola, M., Song, 2014) and the IEA 15 MW semi-submersible (Allen *et al.*, 2020). In Section 3.4, an upscaling methodology for the floating platforms is presented, which is then applied to these two case studies.

3.2.1 OC4 Semi-submersible Model

185 The 5 MW OC4 is a semi-submersible platform with three outer columns, and one central column below the tower, connected with cross braces (Figure 4). The properties are shown in Table 2. Sea water ballast is used within the three columns, with the heave plates filled and the upper part of the column partially filled. The 5 MW reference turbine has a 63 m radius with a rated wind speed of 11.4 m/s. The turbine properties are summarized in Table 3.

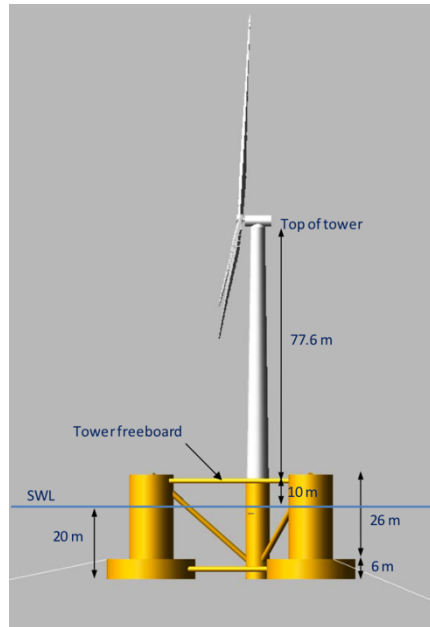


Figure 4: OC4 Platform Dimensions

Table 2: OC4 Platform Properties

Draft	20	m
Heave plate height (H_{hp})	6	m
Freeboard	12	m
Spacing between columns ($Dist_{cc}$)	50	m
Column radius (Rad_{col})	6	m
Heave plate radius (Rad_{hp})	12	m
Ballast density	1,025	kg/m ³
Platform mass including ballast	1.33E+07	kg
$I_{platform}$ about $CM_{platform}$ in pitch	6.827E+09	kgm ²
Platform CM_{system} below waterline	-13.46	m



190

Table 3: 5 MW Reference Turbine Properties (Jonkman *et al.*, 2009)

Rating	5	MW
Rotor radius	63	m
Hub height	90	m
Rated wind speed	11.4	m/s
Rotor mass	110,000	kg
Nacelle mass	240,000	kg
Tower mass	249,718	kg
Specific power	401	W/m ²

The wind turbine is upscaled to 10 MW, 15 MW, and 20 MW using aerodynamic similarity and by holding the specific power (S_p) constant. Specific power is defined as the rated power, P_R , divided by the rotor swept area and is reported in units of W/m² in Eq. (6).

195
$$S_p = \frac{P_R}{\pi R^2} \tag{6}$$

200 The specific power of the original OC4 turbine is 401 W/m². The rotor diameter is calculated for each upscaled turbine rating (Table 4). The tower mass is upscaled by a factor of 2, which is based on the upscaling trends of the reference turbine towers. The rotor nacelle assembly (RNA) mass is upscaled by a factor of 2.2 based on literature on upscaling trends that account for technological advancement (Jamieson, 2018). The hub height is calculated assuming that there is a 30 m gap between the bottom of the rotor plane and the waterline. The methodology for upscaling the platform for each turbine model is presented in Section 3.4.

Table 4: Rotor Radius of Upscaled OC4 Turbines

Power rating (MW)	Rotor radius (m)	Hub height (m)
10	89	119
15	109	139
20	126	156

3.2.2 IEA Semi-submersible Model

205 The IEA 15 MW turbine was designed with both a semi-submersible platform and also a monopile (Allen *et al.*, 2020; Gaertner *et al.*, 2020). The 15 MW IEA semi-submersible platform has three outer columns and one central column to support the turbine (Figure 3). The 20 m draft is the same as the OC4 semi-submersible. Semi-submersible platforms have a relatively

shallow draft compared to a spar platform, and this is prioritized for the 15 MW design which has a 20 meter draft. One noticeable difference between the OC4 and IEA designs is the pontoons between the three columns, instead of heave plates.

210 The IEA 15 MW semi-submersible platform properties are shown in Table 5.

Table 5: IEA 15 MW Semi-submersible Platform Properties (Allen *et al.*, 2020)

Draft	20	m
Freeboard	15	m
Dist _{cc}	89.63	m
Rad _{col}	6.25	m
Pontoon height (H _{pon})	7	m
Platform mass including ballast	1.78E+07	kg
Seawater ballast mass	1.13E+07	kg
Iron-ore ballast mass	4.80E+06	kg
I _{platform} about CM _{platform} in pitch	1.251E+10	kg·m ²
CM _{platform} below waterline	-14.94	m

Table 6: 15 MW Reference Turbine Properties (Gaertner *et al.*, 2020)

Rated power	15	MW
Rotor radius	120	m
Hub height	150	m
Rated wind speed	10.59	m/s
Rotor mass	3.85E+05	kg
Nacelle mass	6.31E+05	kg
Tower mass	1.26E+06	kg
Sp	332	W/m ²

215

Table 7: Rotor Radius of Upscaled IEA Turbines

Power rating (MW)	Rotor radius (m)	Hub height (m)
20	138	168
25	155	185
30	170	200



The 15 MW reference turbine has a rotor radius of 120 m and a rated wind speed of 10.59 m/s. The turbine has a lower specific power of 332 W/m² compared to the 5 MW reference turbine (401 W/m²) because of the lower rated wind speed. The turbine properties are summarized in Table 6. The 15 MW IEA semi-submersible wind turbine is upscaled to 20 MW, 25 MW, and 30 MW. The rotor diameters of the three upscaled turbines are shown in Table 7. Again, the tower mass is upscaled by a factor of 2 and the rotor nacelle assembly (RNA) mass is upscaled by a factor of 2.2. The hub height is calculated assuming that there is a 30 m gap between the bottom of the rotor plane and the waterline.

3.3 Validation of the Hydrodynamic Model for Case Study Turbines

The hydrodynamic model presented in Section 3.1 is validated by simulating the two case study reference turbines in OpenFAST (Jonkman and Buhl, 2005; National Renewable Energy Laboratory, 2020). OpenFAST is used to calculate the static platform pitch under steady, rated wind speed and to calculate the pitch natural period of the system. The OC4 semi-submersible platform result for platform pitch angle is shown in Figure 5, which is estimated as 3.26°. The platform pitch value calculated using the presented hydrodynamic model Eq. (4) is 3.55°. Both platform pitch angles are relative to the waterline. The 9% error is acceptable for the purpose of setting the platform pitch angle for upscaling, especially since the proposed model is much less computationally expensive than OpenFAST.

The natural period of the OC4 semi-submersible is evaluated in OpenFAST by using a free decay test (Figure 6), with an initial platform pitch angle of 8 deg. Based on this test, the natural period of the system of 25.5 s. The published natural period is 27.0 s (Robertson, A., Jonkman, J., Masciola, M., Song, 2014). The pitch natural period of the system calculated using the hydrodynamic model Eq. (5) is 24.2 s, with 10% error relative to the published value and 5% error relative to the natural period found using OpenFAST. The error is likely due to second order effects in OpenFAST that are not captured in the hydrodynamic model.

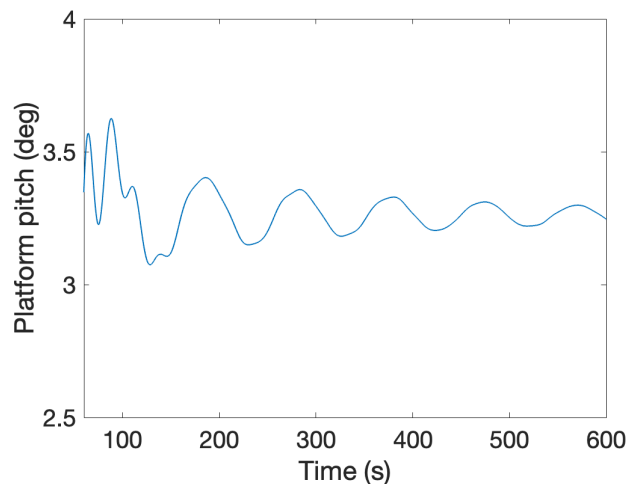


Figure 5: OC4 Platform Pitch Angle at Rated Wind Speed Using OpenFAST

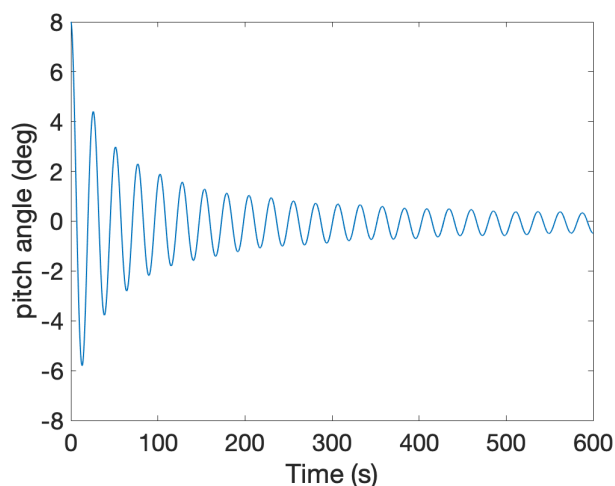


Figure 6: Free Decay of OC4 Semi-submersible Using OpenFAST

240

245

250

OpenFAST is also used to simulate the 15 MW IEA wind turbine with the semi-submersible platform. The static platform pitch angle is estimated as 3.6° at steady, rated wind speed (Figure 7). The platform pitch angle found using the hydrodynamic model Eq. (4) is 4.9° . This 36% error in static pitch angle as compared with the OpenFAST model may be due to limitations in what is known about the IEA 15 MW system. For instance, the system center of mass and moment of inertia is published for the 5 MW OC4 system, but not published for the IEA 15 MW system. The platform pitch angle from the hydrodynamic model can be used as a relative rather than absolute pitch angle in order to constrain the upscaled turbine platform pitch angle. The pitch natural period from the OpenFAST free decay test (Figure 8) is estimated as 27.7 s, the published value is 29.5 s, and the result from the hydrodynamic model is 28.6 s. The model has a 3% error relative to the OpenFAST results and a 3% error relative to the published value. The validation results are summarized in Table 8. The model could be further validated with other simulation software or with data from FOWT pilot projects, but further validation is outside the scope of this paper.

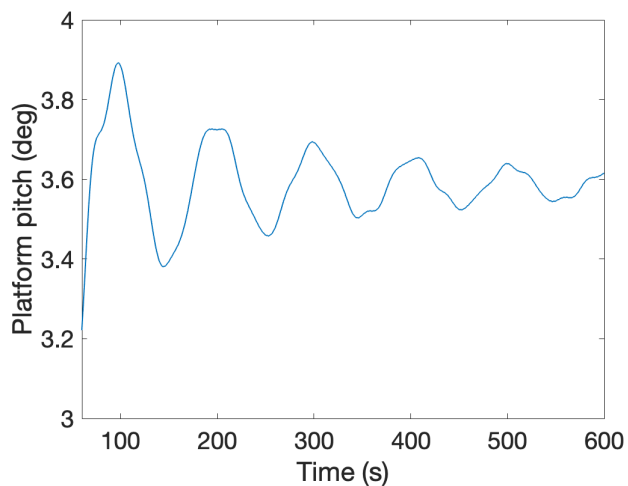


Figure 7: IEA 15 MW Platform Pitch Angle at Rated Wind Speed Using OpenFAST

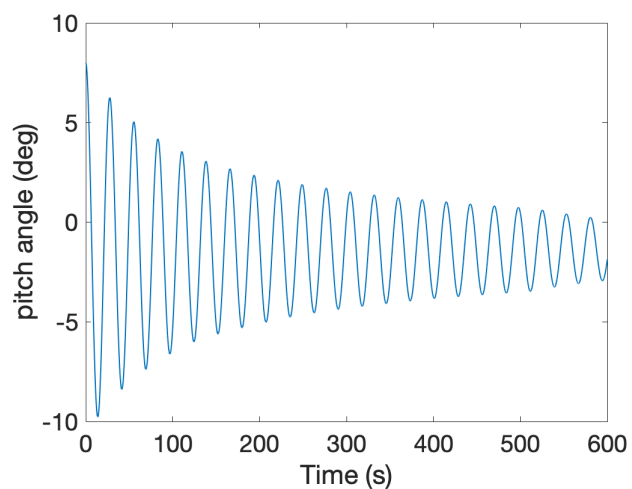


Figure 8: Free Decay of IEA 15 MW Using OpenFAST

255

Table 8: Model Validation

		OC4 5MW	IEA 15MW
Platform pitch angle (deg)	Hydrodynamic model	3.94	4.90
	OpenFAST	3.26	3.60
Pitch natural period (s)	Hydrodynamic model	24.2	28.6
	OpenFAST	25.5	27.7
	Published	27.0	29.5



3.4 Upscaling Methodology

The semi-submersible platforms are upscaled by first upscaling the turbine to a higher power rating, and then using the following methodology for the platforms:

- 260 1. Linearly increase the platform dimensions, specifically the column radii and spacing, with a scaling constant α Eq. (1).
2. Use the hydrodynamic model to find the static pitch angle at rated wind speed Eq. (4) and natural period Eq. (5).
- 265 3. Continue to increase the platform dimensions with the scaling constant α until the upscaled static pitch angle is equivalent to the static pitch angle of the original case study.

This method is effectively a root-finding problem to determine the value of α that results in equal rated platform pitch angles for the baseline and upscaled turbines. The platform dimensions are upscaled uniformly with the scaling constant α in Eq. (1), which is increased in from 0 to 2 in increments of 0.005. The system mass, buoyancy, ballast mass, center of buoyancy, center of mass, static pitch stiffness, static pitch angle, and pitch natural period are calculated for each turbine size (10 - 30 MW) and

270 α scaling constant. In this paper the CM_{system} includes the total system center of mass, including the turbine, tower, and platform. In contrast, the $CM_{platform}$ is used for the platform center of mass, excluding the turbine and tower. The platform pitch stiffness is calculated using Eq. (7), which comes from C_{55} in Eq. (3). The distance from one outer columns to another is $Dist_{cc}$.

$$C_{55} = \rho g \left(\left(V_{disp} (B - CM_{system}) \right) + \frac{\pi}{4} (Rad_{cent})^4 + \frac{3\pi}{4} (Rad_{col})^4 + 2\pi (Rad_{col})^2 \left(\frac{Dist_{cc}}{2} \right)^2 \right) \quad (7)$$

The platform is upscaled until the platform pitch angle at rated wind speed matches the initial design platform pitch angle in

275 Eq. (4). The pitch natural period is calculated using Eq. (8) (derived from Eq. (5)) to ensure that it is not in the predominant wave period range. The added mass coefficient c_A comes from the documentation for each semi-submersible case study (Robertson, A., Jonkman, J., Masciola, M., Song, 2014; Allen *et al.*, 2020). The moment of inertia of the system is I_{system} and the moment of inertia of the platform is $I_{platform}$.

$$T_{55} = \sqrt{\frac{I_{system} + (c_A) (I_{platform})}{c_{55}}} \quad (8)$$

280 3.4.1 OC4 Semi-submersible Upscaling Method

The OC4 semi-submersible turbine is upscaled from 5 MW to 10 MW, 15 MW, and 20 MW. The OC4 platform draft is kept at a constant 20 m and the wall thickness is kept constant at 6 cm. The ballast is sea water with a density of 1025 kg/m³. The center of mass of the entire OC4 system is -10 m, while the center of mass ($CM_{platform}$) of the OC4 platform is -13.46.

The platform displaced volume is set using Eq. (9). The system buoyancy is equal to the mass of the displaced water. The

285 platform steel mass is calculated with the upscaled dimensions, and the ballast mass is the difference between the buoyancy and the steel mass. The radius of the outer columns at the waterline is Rad_{col} , the height of the heave plate on the lower part of the columns is H_{hp} , the radius of the heave plate is Rad_{hp} , and the radius of the central column below the tower is Rad_{cent} .



$$V_{disp} = 3 \left(\pi(Rad_{col})^2(draft - H_{hp}) + \pi(Rad_{hp})^2(H_{hp}) \right) + \pi(Rad_{cent})^2(draft) \quad (9)$$

3.4.2 IEA Semi-submersible Upscaling Method

290 The IEA 15 MW turbine is upscaled to 20 MW, 25 MW, and 30 MW. Since both the 15 MW IEA and the 5 MW OC4 had an
equivalent draft of 20 MW, the OC4 platform upscaling kept the draft constant. However, the IEA platform draft is increased
with α for the larger turbines. The upscaled IEA platform wall thickness is kept at a constant 4.5 cm. The IEA platform has
sea water ballast filling the pontoons and an iron-ore ballast partially filling the columns. The iron-ore ballast density is
estimated to be 4,300 kg/m³. The center of buoyancy, center of mass of the platform, and center of mass of the entire system
295 are calculated. The $CM_{platform}$ of the IEA 15 MW platform is -15 m while the total CM_{system} of the system is -2.8 m.
The displaced volume is calculated using Eq. (10). The platform steel mass, buoyancy mass, and ballast mass are calculated.
The sea water ballast fills up the pontoon inner volume. The remaining ballast mass partially fills the three outer columns with
iron-ore. The column radius for this type of semi-submersible platform is Rad_{col} and the radius of the central column is Rad_{cent} ,
the pontoon length, width, and height are L_{pon} , W_{pon} , and H_{pon} respectively.

$$300 \quad V_{disp} = 3 \left(\pi(Rad_{col})^2(draft) + (L_{pon})(W_{pon})(H_{pon}) \right) + \pi(Rad_{cent})^2(draft) \quad (10)$$

4 Results and Discussion

In this Section, the case study results using the methodology presented in Section 3 are analyzed.

4.1 OC4 Platform Upscaling Results

The platform pitch angle at rated thrust is plotted for each upscale factor value in Figure 9. As the α value increases, the
305 platform dimensions increase, and the static platform pitch angle decreases. The platform pitch angle of the upscaled platforms
matches the OC4 angle of 3.5° at an α of 0.75.

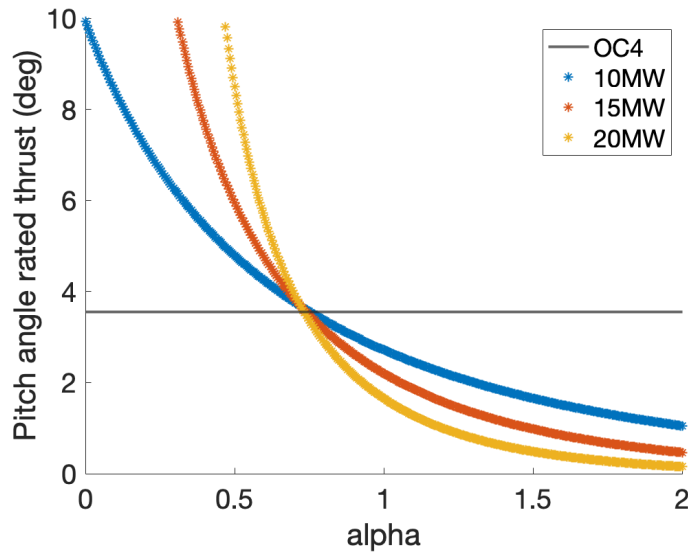


Figure 9: OC4 Platform Pitch Angle of Upscaled Systems at Rated Thrust

310 The natural period of the system is also evaluated using Eq. (8), shown in Figure 10. The pitch natural period is over 20 s for the entire range of α , and is 24.2 s for the baseline OC4 5 MW system. Note that for the 20 MW upscaled system in the $\alpha = 0 - 0.32$ range, the system is unstable. This is because the platform stiffness term becomes negative as the center of mass of the system is raised, with a 20 MW turbine on a platform that is too small.

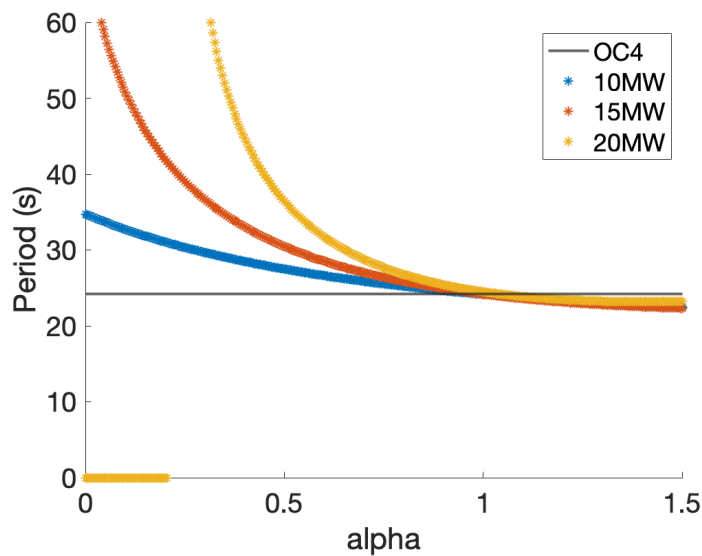


Figure 10: OC4 Natural Period of Upscaled Systems

315

The semi-submersible platform is upscaled from the OC4 design using a scaling factor of $\alpha = 0.75$, which is the approximate value that preserves the static platform pitch angle at rated thrust. The results are shown in Table 9. The specific power, draft,



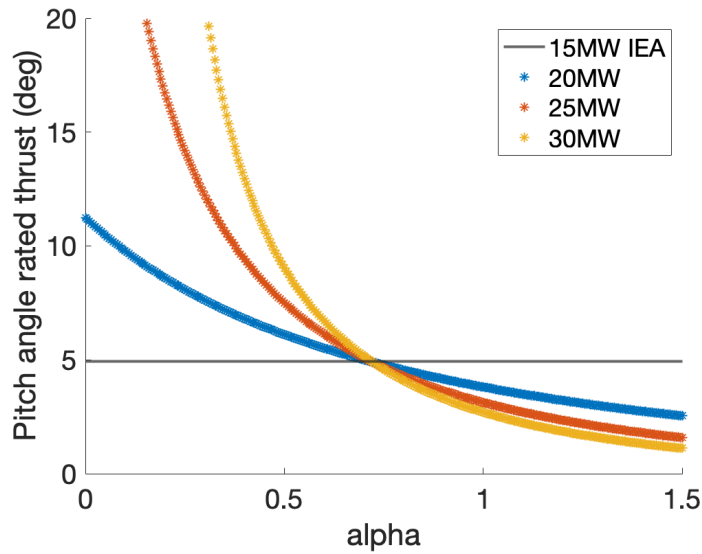
320 wall thickness, and platform pitch angle are kept constant. The moment of inertia is shown for the entire system including the tower and RNA. The ratio of platform steel mass to total platform mass decreases from 27% for the OC4 turbine to 18% for the 20 MW upscaled system. Fitting a curve to the mass data indicates that the platform steel mass is upscaled by $R^{1.3}$ and the total platform mass is upscaled by $R^{1.8}$. The ballast mass is increasing more quickly than the steel mass, and ballast mass is significantly cheaper. The natural period of the system in pitch increases slightly as it is upscaled.

Table 9: Upscaled OC4 Table of Results

Rated Power	MW	5	10	15	20
Sp	W/m ²	401	401	401	401
Rotor radius (R)	m	63	89	109	126
Draft	m	20	20	20	20
CM _{platform}	m	-13.6	-13.1	-12.5	-12.0
CM _{system}	m	-10	-7.9	-6.1	-4.6
Pitch angle	deg	3.5	3.5	3.4	3.3
Total stiffness	Nm/rad	1.0E+09	2.7E+09	4.9E+09	7.6E+09
I _{system}	kgm ²	1.1E+10	3.5E+10	7.0E+10	1.2E+11
Pitch Natural period	s	24.2	26.4	27.7	28.7
Natural frequency	Hz	0.26	0.24	0.23	0.22
Steel mass	kg	3.59E+06	5.60E+06	7.30E+06	8.86E+06
Ballast mass	kg	9.70E+06	2.0E+07	3.0E+07	4.0E+07
Total platform mass	kg	1.3E+07	2.5E+07	3.7E+07	4.9E+07
Percent steel mass		27%	22%	20%	18%

325 4.2 IEA Platform Upscaling Results

Figure 11 shows the static platform pitch angle at rated thrust for each α increment for the IEA 15 MW upscaled platform. The platform dimensions increase with α , and so the static platform pitch angle decreases. The platform pitch angle of the upscaled platforms matches the 15 MW IEA pitch value of 4.9° for the IEA 15 MW at $\alpha = 0.72$, similar to the OC4 upscaling.



330

Figure 11: IEA 15 MW Platform Pitch of Upscaled Systems at Rated Thrust

The natural period is also calculated at each upscaling factor increment using Eq. (8). The pitch natural period for the 20 MW, 25 MW, and 30 MW is shown in Figure 12. The pitch natural period is over 20 s for the entire upscaling range of α . The pitch natural period for the baseline IEA 15 MW platform is 28.6 s. Again, the platform becomes unstable for the 30 MW turbine in the $\alpha = 0 - 0.18$ range because of the high center of mass of the system with the relatively small platform.

335

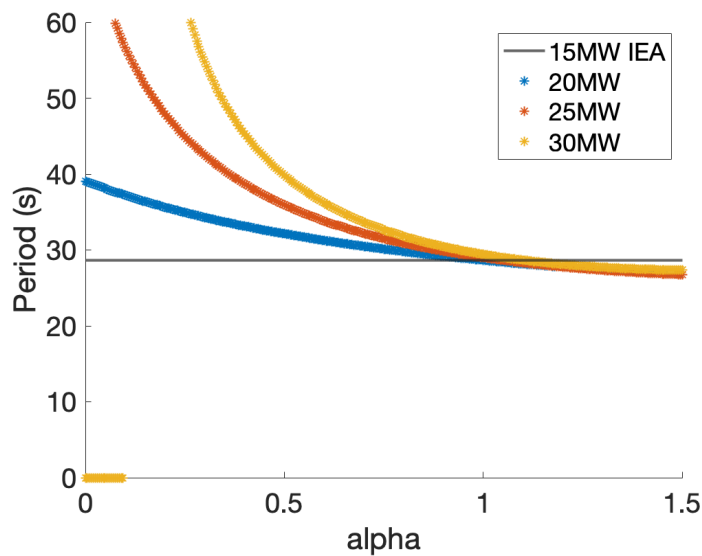


Figure 12: IEA Natural Period of Upscaled Systems

The semi-submersible platforms are upscaled from the IEA design using a scaling factor of $\alpha = 0.72$ for the platform dimensions, shown in Table 10. The 332 W/m^2 specific power, 4.5 cm wall thickness, and 5.9° platform pitch angle are kept constant. The ratio of platform steel mass to total platform mass is reduced as the turbines are upscaled; the 15 MW IEA system has 19% steel mass, and the 30 MW IEA system has 19% steel mass compared to total platform mass including ballast. Fitting a curve to the mass data indicates that the platform steel mass is upscaled by $R^{1.4}$ and the total platform mass is also upscaled by $R^{2.2}$. The natural period of the system in pitch increases slightly as it is upscaled.

Table 10: Upscaled IEA 15 MW Table of Results

Rated Power	MW	15	20	25	30
Sp	W/m ²	332	332	332	332
Rotor radius	m	120	138	155	170
Draft	m	20.0	22.1	24.0	25.7
CM_{platform}	m	-16.8	-18.6	-20.2	-21.6
CM_{system}	m	-5	-5.5	-5.8	-6.1
Platform pitch	deg	4.9	4.9	4.9	4.9
Total stiffness	Nm/rad	3.3E+09	4.9E+09	6.8E+09	8.8E+09
I_{system}	kgm ²	5.3E+10	8.9E+10	1.4E+11	1.9E+11
Pitch Natural period	s	28.6	30.3	31.9	33.2
Natural frequency	Hz	0.22	0.21	0.20	0.19
Steel mass	kg	3.5E+06	4.7E+06	6.0E+06	7.3E+06
Seawater ballast mass	kg	5.7E+06	7.7E+06	1.0E+07	1.2E+07
Fixed ballast mass	kg	9.2E+06	1.3E+07	1.6E+07	2.0E+07
Total platform mass	kg	1.8E+07	2.5E+07	3.2E+07	3.9E+07
Percent steel mass		19%	19%	19%	19%

4.3 Case Study Discussion

Upscaling of both platforms can be compared, specifically at 20 MW. Table 11 shows the comparison between the designs, including the lower specific power and larger rotor radius of the IEA 20 MW system. The upscaled 20 MW IEA platform has a larger draft, smaller wall thickness, higher CM_{system} , and larger static platform pitch angle, whereas the upscaled 20 MW OC4 platform has a larger stiffness, moment of inertia, steel mass, and total platform mass. The pitch natural period and ratio of platform steel mass to total steel mass is similar for both designs. The 5 MW OC4 reference platform was designed in 2014 (Robertson, A., Jonkman, J., Masciola, M., Song, 2014) while the IEA 15 MW platform was designed in 2020 (Allen *et al.*, 2020), which likely explains the reduction in platform steel mass and wall thickness in the more recent design. The IEA



355 platform steel mass scales by $R^{1.4}$ while the OC4 platform steel mass scales by $R^{1.2}$, and the IEA platform steel mass increases more rapidly in part because the draft is increasing while the OC4 draft is constant.

Table 11: Comparison of Upscaled 20 MW IEA with Upscaled 20 MW OC4 System

		Upscaled IEA 20 MW	Upscaled OC4 20 MW
Sp	W/m ²	332	401
Rotor radius	m	138	126
Draft	m	22.1	20
Wall thickness	m	0.045	0.06
Dist _{cc}	m	100	84
CM _{platform}	m	-16.7	-11.7
CM _{system}	m	-5.0	-4.8
Pitch angle	deg	4.9	3.5
Total stiffness	Nm/rad	4.9E+09	7.6E+09
I _{system}	kg-m ²	8.9E+10	1.2E+11
Pitch Natural period	s	30.3	28.7
Steel mass	kg	4.8E+06	8.9E+06
Seawater ballast mass	kg	7.8E+06	4.0E+07
Fixed ballast mass	kg	1.2E+07	0
Total platform mass	kg	2.5E+07	4.9E+07
Steel mass ratio		19%	18%

360 The case studies can be used to understand upscaling trends for floating platforms. Comparing four of the 5 MW OC4 systems with one upscaled 20 MW OC4 system, the total platform mass including ballast is similar, within 8%, however the platform steel mass is reduced by up to 38% for the single 20 MW turbine case. There is a lower ratio of platform steel mass to total platform mass for the upscaled platforms, primarily because the wall thickness remains constant. Rotor power scales with R^2 , and so turbine power will increase more rapidly than platform steel mass as the OC4 turbines are upscaled to the $R^{1.3}$. Additionally, the ballast mass does increase for the upscaled systems, but the ballast cost is likely significantly lower.

365 Comparing two 15 MW IEA systems with one upscaled 30 MW IEA system, the total platform mass including ballast is similar within 6% of the mass of the 30 MW upscaled design. Additionally, the platform steel mass is 21% lower for one 30 MW system as compared with two 15 MW systems. The IEA platform mass scales to $R^{1.4}$, and so the platform power will scale more quickly than steel mass. This result suggests that there are advantages to continued upscaling of turbines on floating platforms, specifically when the platform draft and wall thickness are kept constant.



370 It is notable that the static pitch angle of the platform varies for each case study design. The OC4 semi-submersible static pitch angle is 3.6° and the IEA semi-submersible static pitch angle is 4.9°. Early FOWTs had a small static pitch angle to be conservative in design, but there are no absolute standards on what value of static pitch angle is acceptable.

The upscaling methodology is useful to identify trends for each platform type, but it should be noted that the designs are not being optimized. The original designs (OC4 and IEA 15 MW) are not optimized initially, but are designed based on expertise. The upscaled designs are also not optimized, so it is possible that other platform designs may be more stable with less platform steel mass. Optimization studies can be conducted for individual projects at specific sites, or for future research projects, but are outside the scope of this research study. Future work will also estimate levelized cost of energy (LCOE) for the upscaled turbines.

4.4 Comparison of Platform Upscaling with Similar Studies for the OC4 Platform

380 The upscaled OC4 semi-submersible design can also be compared to other semi-submersible upscaling studies (George, 2014; Leimeister *et al.*, 2016; Kikuchi and Ishihara, 2019a). These upscaling studies do not seek to find platform scaling relations, but instead upscale one specific design. As stated previously, Leimeister *et al.* (Leimeister *et al.*, 2016) upscales the OC4 to a 7.5 MW semi-submersible, George (George, 2014) upscales OC4 to a 10 MW semi-submersible, and Kikuchi and Ishihara (Kikuchi and Ishihara, 2019a, 2019b) upscale the Fukushima FORWARD design to both a 7.5 MW and 10 MW semi-submersible. Table 12 shows the 7.5 MW semi-submersible upscaling results and Table 13 shows the 10 MW semi-submersible upscaling results. Both tables include the upscaled OC4 platform from this study.

Table 12: 7.5 MW Upscaled Semi-submersible Comparison

		Leimeister (2016)	% difference from this study	George (2014)	% difference from this study	This study
Draft	m	24.5	23%	20	0%	20
Wall thickness	m	0.078	29%	0.060	0%	0.060
Rad _{col}	m	7.4	5%	6.8	-3%	7.0
Rad _{hp}	m	14.7	5%	13.6	-3%	13.9
Dist _{cc}	m	61.3	5%	56.5	-3%	58.1
Static pitch angle	deg	3.7	-6%	2.4	-39%	3.9
Pitch natural period	s	34.1	34%	25.0	-2%	25.5



390

Table 13: 10 MW Upscaled Semi-submersible Comparison

		George (2014)	% difference from this study	Kikuchi (2019)	% difference from this study	This study
Draft	m	20	0%	21.3	7%	20
Wall thickness	m	0.060	0%	0.060	0%	0.060
Rad _{col}	m	7.6	-3%	8.0	3%	7.8
Rad _{hp}	m	15.1	-3%	16.0	3%	15.5
Dist _{cc}	m	63.0	-3%	54.3	-16%	64.8
Static pitch angle	deg	3.1	-18%	4.5	20%	3.8
Pitch natural period	s	28.0	6%	26.0	-1%	26.4

All studies upscale the platform based on the increase in power rating. George (George, 2014) and Kikuchi and Ishihara (Kikuchi and Ishihara, 2019a, 2019b) limit certain dimensions such as draft and platform wall thickness, and all check criteria to ensure the design meets natural period and static pitch angle requirements. Leimeister et al. (Leimeister *et al.*, 2016) upscales the platform dimensions conservatively with $\alpha = 1$. In contrast, George (George, 2014) and Kikuchi and Ishihara (Kikuchi and Ishihara, 2019a, 2019b) both use the RNA mass upscaling ratio in order to set the upscaling factor for the platform. George uses an upscaling factor of $\alpha = 0.6$, which is why the results are less conservative than for Leimeister et al. (Leimeister *et al.*, 2016). This research proposes using $\alpha = 0.75$.

The platform dimensions of this study are within 3% of the results for George (George, 2014) for all platform dimensions shown. The only notable difference is that the calculated static pitch angle is lower for George (George, 2014) even though the platform is slightly smaller than the one modeled in this study. The Leimeister et al. (Leimeister *et al.*, 2016) study is the only one that increases both the draft and wall thickness with upscaling. Additionally, the platform pitch natural period is 34% larger for Leimeister et al. (Leimeister *et al.*, 2016) due to the larger platform dimensions. Finally, the Kikuchi and Ishihara (Kikuchi and Ishihara, 2019a, 2019b) study has a 16% smaller distance between the outer columns, which causes an increase in the static pitch angle.

Overall, the Leimeister et al. (Leimeister *et al.*, 2016) study is the most conservative, the George (George, 2014) study is the most similar to the method proposed here, and the Kikuchi and Ishihara (Kikuchi and Ishihara, 2019a, 2019b) study increases the draft but reduces the spread between columns. The spread between the columns provides the largest contribution to stability for the semi-submersible platform type, so this reduction in column spread may have drawbacks.

This proposed upscaling method differs from the other methods in that there is one platform dimension upscaling factor identified, which can be used in Eq. (1) to upscale any semi-submersible platform. This is in contrast to the other studies which upscale one specific case study through a variety of methods that include some trial and error, and do not result in a scaling factor.



4.5 Analytical Model for Semi-submersible Platform Upscaling

415 There are classical analytical scaling laws for wind turbines (Manwell, McGowan and Rogers, 2009), but the scaling laws for
 FOWT platforms are not fully understood. The results from the case studies can be used develop analytical upscaling relations
 for the semi-submersible platforms. For the static pitch angle to match the original semi-submersible design, an upscale factor
 of approximately $\alpha = 0.72 - 0.75$ was found for both the OC4 5 MW and IEA 15 MW designs. Additionally, the platform steel
 mass scales with $R^{1.3} - R^{1.4}$ when the wall thickness is kept constant, but would scale to a greater ratio if the wall thickness
 420 increases proportionally with R . Thus, the upscaling is more advantageous in terms of platform steel mass when the wall
 thickness is kept constant. These results have been determined using hydrodynamic models and an iterative method, but
 fundamental equations for the static pitch when upscaling can also be derived analytically. The static pitch equation is shown
 in Eq. (11), which is an expanded version of Eq. (4).

$$\theta_p = \frac{M_{aero}}{(\rho g W_{55} + \rho g V_{disp}(B - CM_{system}))} \quad (11)$$

425 The numerator is the aerodynamic moment on the platform at rated wind speed, which is the thrust of the wind turbine
 multiplied by the distance between the rotor hub and the center of mass of the system. The denominator of the equation is the
 platform stiffness $C_{55}^{hydrostatics}$. The mooring stiffness is neglected in these calculations; Section 4.3 addresses this assumption
 with a sensitivity study. The platform stiffness includes two terms, one is based on buoyancy ($V_{disp}(B - CM_{system})$) and the other
 on waterplane area (W_{55}). The waterplane area term provides the dominant stability for semi-submersible platforms,
 430 contributing 94% for the 15 MW IEA. Literature shows that the buoyancy term is always small for semi-submersible platforms,
 and other research studies have neglected the buoyancy term in the stiffness equation for semi-submersible upscaling (Kikuchi
 and Ishihara, 2019a). For both the OC4 and IEA semi-submersible platforms, the buoyancy term is actually destabilizing
 because the turbine and tower mass raise the CM_{system} above position B . Eq. (11) can be simplified to Eq. (12) by neglecting
 the buoyancy term and only considering the waterplane area term in the denominator.

$$435 \theta_{p,s} = \left[\frac{Th \times h}{\rho g W_{55}} \right]_{original} = \left[\frac{Th \times h}{\rho g W_{55}} \right]_{new} \quad (12)$$

There is aerodynamic similarity between the original and upscaled turbine with constant density of air, thrust coefficient, and
 rated wind speed. The thrust is Th and h is the distance between the hub and the CM_{system} . For simplicity, the hub height is used
 and the distance from the CM_{system} and the waterline is neglected. The hub height is 90% of the total distance for the OC4 and
 98% for the IEA 15 MW designs. Additionally, the hub height is defined as 1.25 times the rotor radius in this model. This
 440 gives the 30 m clearance for the 15 MW IEA turbine and increases the clearance for larger turbines. The second moment area
 of the waterplane for the IEA semi-submersible is calculated using Eq. (13), which is also shown in a simplified version in Eq.
 (14).

$$W_{55} = \frac{\pi}{4} [Rad_{cent}^4 + 3(Rad_{col})^4] + 2\pi(Rad_{col})^2(8.28 * \sin 60 * Rad_{col})^2 \quad (13)$$

$$W_{55} = \frac{\pi}{4} (Rad_{cent})^4 + \left(\frac{3\pi}{4}\right) (138)(Rad_{col})^4 \quad (14)$$



445 Calculating W_{55} for the 15MW IEA platform, the first term (central column) is 0.1% of the total and the second term (three outer columns) is 99.9%, indicating that nearly all of the stability comes from the three outer columns. Thus, the first term is neglected and only the column radius term is considered. The thrust and hub height equations are shown in Eq. (15). The rotor diameter is defined as ϕ , with $\phi_{original}$ as the original rotor diameter and ϕ_{new} as the rotor diameter of the upscaled turbine.

$$\frac{\left(\frac{1}{2}\rho\alpha\pi\left(\frac{\phi_{original}}{2}\right)^2 C_{T}u^2\right)\left(1.25*\left(\frac{\phi_{original}}{2}\right)\right)}{103.6\pi(Rad_{col_original})^4} = \frac{\left(\frac{1}{2}\rho\alpha\pi\left(\frac{\phi_{NEW}}{2}\right)^2 C_{T}u^2\right)\left(1.25*\left(\frac{\phi_{NEW}}{2}\right)\right)}{103.6\pi(Rad_{col_NEW})^4} \quad (15)$$

450 Note that any semi-submersible with three outer columns would reduce to the same equation, because the coefficient terms cancel out. Eq. (15) can be further simplified to only include the column radius and rotor diameter Eq. (16).

$$\frac{(\phi_{original})^3}{(Rad_{col_original})^4} = \frac{(\phi_{NEW})^3}{(Rad_{col_NEW})^4} \quad (16)$$

This scaling relation for the semi-submersible platform can determine the column radius needed for an upscaled semi-submersible platform based on the original column radius, and the diameter of the original and upscaled turbines. Eq. (17) is in a similar format to the generic scaling relation shown in Eq. (1). The scaling factor between the upscaled column radius and the original column radius is $\alpha = 0.75$, which is very similar to the upscaling factor of $\alpha = 0.72-0.75$ that was found for the semi-submersible case studies. Thus, the analytical formulation recovers the same upscaling factor as the more complex hydrodynamic model.

$$Rad_{col_NEW} = (Rad_{col_original}) * \left[\frac{\phi_{NEW}}{\phi_{original}}\right]^{3/4} \quad (17)$$

460 This relation is similar to the square-cube law of blade upscaling, except that it shows that platform upscaling is likely to be advantageous because platform stiffness scales faster than wind turbine overturning moment. The upscaled column radius scales at $\alpha = 0.75$ because the overturning moment from rated thrust is proportional to the diameter cubed, and the stiffness is dominated by the column radius to the fourth power. This only defines column radius and column spread, but all parameters can be upscaled by the same α of 0.75 for a semi-submersible upscaled design. Additionally, if it is assumed that all semi-submersible platform dimensions increase, including wall thickness and draft, the platform steel mass increases by a factor of 2.25 in Eq. (18). However, if the platform wall thickness is kept constant, as it was in the case studies, the platform steel mass increases by a factor of 1.5. If multiple small FOWTs were used instead of upscaling, the steel mass would scale as R^2 .

$$M_{platform_NEW} = (M_{platform_original}) * \left[\frac{\phi_{NEW}}{\phi_{original}}\right]^{1.5} \quad (18)$$

4.6 Sensitivity Studies

470 The results presented above rely on a variety of assumptions, which are now assessed using parameter sensitivity studies.

4.6.1 Mooring Line Sensitivity

This research assumes that the stiffness contributions from the mooring lines can be neglected for the first-order platform pitch angle calculations. A mooring line sensitivity study is conducted to evaluate the contribution of mooring line stiffness to



platform pitch motion. The study uses the OC4 system using OpenFAST and evaluates the natural period of the system when the mooring line stiffness is reduced. The published natural period of the system is 27 s. OpenFAST is run with the tower degrees of freedom off, and the pitch natural period is calculated using a free decay test (Figure 13-Figure 14). The mooring line stiffness (EA) is then decreased from the original stiffness value to a stiffness that is one-eighth of the original value. The natural period is calculated for each simulation to determine the impact on the system dynamics. Table 14 shows that reducing the mooring line stiffness by a factor of eight reduces the pitch natural period of the system by less than 1%.

480

Table 14: Pitch Natural Period of OC4 with Reduced Mooring Line Stiffness

EA (MN)	Tn (s)
753.6	25.535
502.4 (/1.5)	25.5625
376.8 (/2)	25.590
188.4 (/4)	25.645
94.2 (/8)	25.740

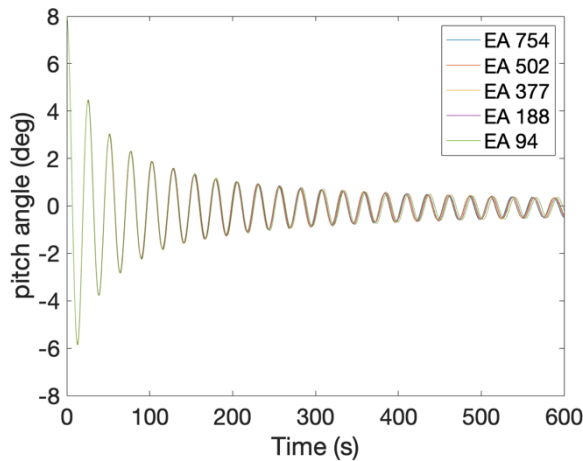


Figure 13: Free Decay Test for OC4

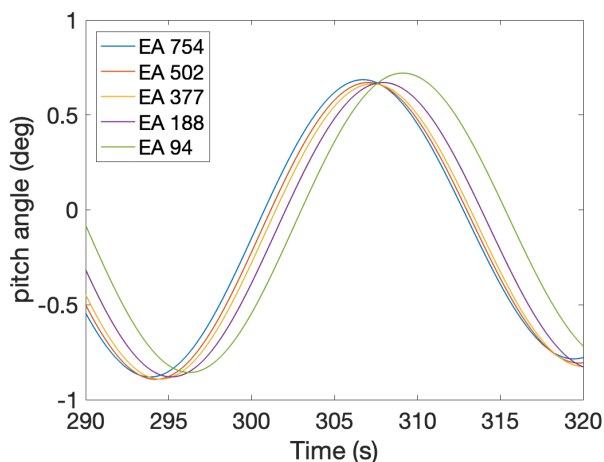


Figure 14: Free Decay Test of OC4 for 30 second Interval

485

The static pitch angle at rated thrust can also be evaluated in OpenFAST while decreasing the mooring line stiffness. OpenFAST is run for the OC4 system at steady, rated wind speed (Figure 15). Table 15 shows that when the mooring line stiffness is reduced by a factor of eight, the static pitch angle is increased by less than 1%. Thus, while mooring design may change as platform size increases, these results indicate that the mooring stiffness has negligible impact on the platform dynamics, and so can be ignored in upscaling studies. Further analysis of mooring line behavior is therefore outside the scope of this research.

490

Table 15: Static Pitch Angle of OC4 with Mooring Stiffness

EA (MN)	Pitch angle (deg)
753.6	3.2592
502.4 (/1.5)	3.2618
376.8 (/2)	3.2636
188.4 (/4)	3.2729
94.2 (/8)	3.2809

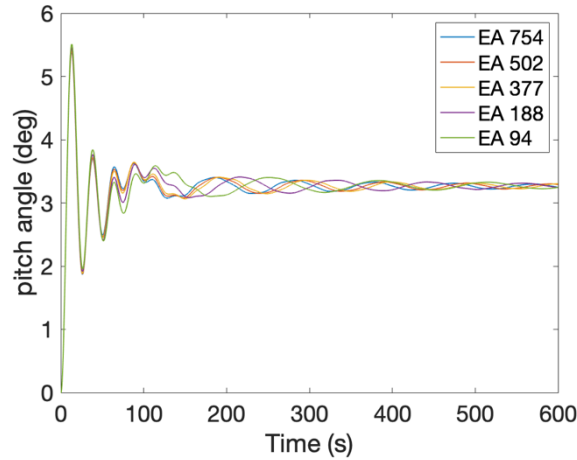


Figure 15: Static Pitch of OC4 at Rated Thrust with Mooring Line Stiffness

495

4.6.2 Rotor Nacelle Assembly Mass Sensitivity

The upscaling case studies are conducted with an assumption about the mass scaling of the rotor nacelle assembly (RNA). Classical upscaling uses R^3 scaling of RNA mass, while scaling based on data results in $R^{2.2}$ scaling approximately. In addition to the impact on turbine mass, the change in RNA mass scaling also impacts the FOWT platform design, mass, and cost. While some researchers have focused on reducing turbine mass to reduce the size and cost of the platform (Jacob C. Ward, Andrew J. Goupee, Anthony M. Viselli, 2021), it is still unclear if RNA mass reduction is a major design driver for FOWT design. An RNA mass sensitivity study is conducted for the IEA 15 MW wind turbine. The RNA mass is reduced to 50% of the original mass, while the tower mass remains constant. As the RNA mass decreases, the platform size is reduced so that the platform pitch angle at rated thrust remained constant. Table 16 shows the results of the RNA mass sensitivity study for the 15 MW IEA semi-submersible.

505

Table 16: RNA Mass Sensitivity Results for IEA 15 MW

RNA mass reduction	RNA mass	Platform pitch angle	CM	Total stiffness	Steel mass	Steel mass reduction	Total platform mass	Platform mass reduction
	kg	deg	m	Nm/rad	kg	%	kg	%
original	1.02E+06	7.8	-2.7	2.77E+09	3.88E+06		1.84E+07	
5%	9.66E+05	7.6	-3.1	2.86E+09	3.88E+06	0%	1.85E+07	0%
15%	8.64E+05	7.8	-3.4	2.81E+09	3.81E+06	-2%	1.79E+07	-3%
29%	7.19E+05	7.7	-4.1	2.85E+09	3.73E+06	-4%	1.75E+07	-5%
42%	5.87E+05	7.7	-4.8	2.87E+09	3.65E+06	-6%	1.70E+07	-7%
50%	5.09E+05	7.9	-5.1	2.81E+09	3.58E+06	-8%	1.65E+07	-10%



510 The results show that the CM_{system} lowers with the reduced RNA mass. A smaller platform is also needed to support the smaller RNA mass (because of the lower center of mass). The platform steel mass is reduced by 8% (300,000 kg) when the RNA mass is reduced by 50% (510,000 kg) and the total platform mass including ballast is reduced by 10%. The waterplane area component of the platform stiffness is stabilizing, while the contribution from the center of mass is destabilizing; thus, when the RNA mass is reduced by 50%, the destabilizing stiffness term is reduced by 35%.

5 Conclusion

515 In Floating offshore wind turbines are being developed to harness energy in windy, deep-water sites. While individual floating platform designs can be optimized for a specific site, this research provides fundamental insight that can guide technology development by creating a generalized methodology for semi-submersible platform upscaling. This work has resulted in an upscaling factor for semi-submersible platform dimensions and mass that is comparable to the classical turbine scaling relations (Manwell, McGowan and Rogers, 2009).

520 The numerical method used in the methodology was validated using OpenFAST. The upscaled platform results are closest to those of George (George, 2014), but the results do differ from (George, 2014; Leimeister *et al.*, 2016; Kikuchi and Ishihara, 2019a; Ju *et al.*, 2020), because there is a generic semi-submersible platform dimension upscaling factor presented for all semi-submersible turbines. Additionally, this study differs from the generic semi-submersible scaling study conducted by Wu and Kim (Wu and Kim, 2021), because their method is an iterative approach to find the column radius and spread for a semi-submersible, and there is no scaling factor provided.

525 Two upscaling case studies are evaluated: the OC4 semi-submersible turbine is upscaled from 5 MW to 20 MW and the IEA 15 MW semi-submersible turbine is upscaled from 15 MW to 30 MW. The semi-submersible scale factor for both case studies is approximately $\alpha = 0.75$, using both numerical and analytical methods. These relations can be used to quickly estimate the platform dimensions for a larger turbine rotor. Additionally, the analytical solution shows that platform steel mass increases with $R^{1.5}$ when platform wall thickness is kept constant using the upscaling method, and R^2 when multiple, smaller FOWTs are used instead of upscaling.

530 Future work should validate the upscaled FOWT designs using OpenFAST, which involves creating a turbine and platform model for each upscaled design. A better understanding of the upscaled designs in extreme wind and wave conditions can further the knowledge of platform upscaling. An additional area of future work is to conduct cost of energy analysis, in order to gain insight into how turbine and platform scaling impact the system economics. Upscaling the platform with a constant wall thickness causes the platform steel mass to increase with a factor of approximately $R^{1.5}$, suggesting that larger turbines may be advantageous. But a more nuanced and detail analysis is needed, which includes balance of system costs and estimates on annual energy production, to assess the likely impact of continued upscaling of FOWTs. The upscaling of FOWT systems is already taking place in industry, and better understanding of platform scaling can give key insight into research and industry development.



References

- 540 Ågotnes, A. *et al.* (2013) *Deep water: The next step for offshore wind*. Brussels, Belgium: The European Wind Energy Association (EWEA). Available at: https://www.researchgate.net/publication/257553940_Deep_Water_The_next_step_for_offshore_wind_energy_A_report_by_the_European_Wind_Energy_Association.
- Allen, C. *et al.* (2020) *Definition of the UMaine VoltturnUS-S Reference Platform Developed for the IEA 15MW Wind Turbine*. Golden, CO. Available at: <https://www.nrel.gov/docs/fy20osti/76773.pdf>.
- 545 Ashuri, T. (2012) *Beyond Classical Upscaling : Integrated Aeroservoelastic Design and Optimization of Large Offshore Wind Turbines*. Delft University of Technology. doi: 10.4233/uuid:d10726c1-693c-408e-8505-dfca1810a59a.
- Beaubouef, B. (2020) *WindFloat Atlantic represents major offshore wind milestone, Offshore*. Available at: <https://www.offshore-mag.com/renewable-energy/article/14188688/windfloat-atlantic-represents-major-offshore-wind-milestone>.
- 550 Beiter, P. *et al.* (2016) “A Spatial-Economic Cost- Reduction Pathway Analysis for U.S. Offshore Wind Energy Development from 2015–2030,” *National Renewable Energy Laboratory (NREL)*, (September), p. 214.
- Beiter, P. *et al.* (2020) *The Cost of Floating Offshore Wind Energy in California Between 2019 and 2032*. Golden, CO. Available at: <https://www.nrel.gov/docs/fy21osti/77384.pdf>.
- 555 California Energy Commission (2021) *Offshore Renewable Energy*. Available at: <https://www.energy.ca.gov/programs-and-topics/topics/renewable-energy/offshore-renewable-energy>.
- Conversation, T. (2021) *California is planning floating wind farms offshore to boost its power supply - here's how they work*. Available at: <https://theconversation.com/california-is-planning-floating-wind-farms-offshore-to-boost-its-power-supply-heres-how-they-work-163419>.
- 560 Delhommeau, G. (1993) *Numerical Simulation of Hydrodynamics: Ships and Offshore Structures: Seakeeping codes AQUADYN and AQUAPLUS*. Nantes, France.
- Det Norske Veritas Germanischer Lloyd (2017) “DNVGL-RP-C205: Environmental Conditions and Environmental Loads,” *DNV GL Recommended Practice*, (DNVGL-RP-C205), pp. 1–259.
- Duarte, T. M., Sarmiento, A. J. and Jonkman, J. (2014) “Effects of second-order hydrodynamic forces on floating offshore wind turbines,” *32nd ASME Wind Energy Symposium*, (April). doi: 10.2514/6.2014-0361.
- 565 Durakovic, A. (2021) *Largest Floating Offshore Wind Farm Stands Complete, offshoreWind.biz*. Available at: <https://www.offshorewind.biz/2021/08/24/largest-floating-offshore-wind-farm-stands-complete/>.
- Equinor (2021) *Hywind Scotland*. Available at: <https://www.equinor.com/en/what-we-do/floating-wind/hywind-scotland.html>.
- 570 Fukushima Offshore Wind Consortium (no date) *Fukushima Floating Offshore Wind Farm Demonstration Project*. Available at: <http://www.fukushima-forward.jp/english/>.



- Gaertner, E. *et al.* (2020) *Definition of the International Energy Agency 15-Megawatt Offshore Reference Wind Turbine*. Golden, CO. Available at: <https://www.nrel.gov/docs/fy20osti/75698.pdf>.
- GE Renewable Energy (2023) *Haliade-X Offshore wind turbine*. Available at: <https://www.ge.com/renewableenergy/wind-energy/offshore-wind/haliade-x-offshore-turbine>.
575
- George, J. (2014) *WindFloat design for different turbine sizes*. Instituto Superior Tecnico.
- Jacob C. Ward, Andrew J. Goupee, Anthony M. Viselli, H. J. D. (2021) “Experimental investigation into the dynamic behavior of a floating offshore wind turbine stabilized via a suspended counterweight,” *Ocean Engineering*, 228.
- Jamieson, P. (2018) “Upscaling of Wind Turbine Systems,” in *Innovation in Wind Turbine Design*. second. John Wiley & Sons, Ltd., pp. 97–126.
580
- Jonkman, J. M., Matha, D. (2011) “Dynamics of offshore floating wind turbines-analysis of three concepts,” *Wind Energy*, (14), pp. 557–569.
- Jonkman, J. *et al.* (2009) *Definition of a 5-MW reference wind turbine for offshore system development*. Golden, CO. Available at: <https://www.nrel.gov/docs/fy09osti/38060.pdf>.
- Jonkman, J. (2019) “OpenFAST: An Open-Source Tool for Wind Turbine Physics-Based Engineering Modeling,” in *North American Wind Energy Academy (NAWEA)/WindTech 2019*. Amherst, MA.
585
- Jonkman, J. M. (2007) *Dynamics modeling and loads analysis of an offshore floating wind turbine*. Golden, CO: National Renewable Energy Laboratory.
- Jonkman, J. M. and Buhl, M. L. (2005) *FAST User’s Guide*. Golden, CO. doi: 10.2172/15020796.
- Ju, S. *et al.* (2020) “Study of optimal large-scale offshore wind turbines,” *Renewable Energy*, (154), pp. 161–174.
590
- Karimirad, M. (2014) *Offshore Energy Structures*, Springer. Springer International Publishing. doi: 10.1007/978-3-319-12175-8.
- Kikuchi, Y. and Ishihara, T. (2019a) “Upscaling and levelized cost of energy for offshore wind turbines supported by semi-submersible floating platforms,” *Journal of Physics: Conference Series*, 1356(1), pp. 0–12. doi: 10.1088/1742-6596/1356/1/012033.
595
- Kikuchi, Y. and Ishihara, T. (2019b) “Upscaling and levelized cost of energy for offshore wind turbines supported by semi-submersible floating platforms,” in *EERE DeepWind Conference*. doi: 10.1088/1742-6596/1356/1/012033.
- Kikuchi, Y. and Ishihara, T. (2020) “Comparison of dynamic response and levelized cost of energy on three platform concepts of floating offshore wind turbine systems,” *Journal of Physics: Conference Series*, 1452(1). doi: 10.1088/1742-6596/1452/1/012035.
600
- Leimeister, M. *et al.* (2016) “Rational Upscaling of a Semi-submersible Floating Platform Supporting a Wind Turbine,” *Energy Procedia*. The Author(s), 94(January), pp. 434–442. doi: 10.1016/j.egypro.2016.09.212.
- Manwell, J. F., McGowan, J. G. and Rogers, A. L. (2009) *Wind Energy Explained Theory, Design, and Application*. Second Edi, Wiley. Second Edi. Chichester, West Sussex, United Kingdom: John Wiley & Sons, Ltd. doi: 10.1016/B978-0-12-804448-3/00004-9.
605



- Musial, W. *et al.* (2016) *2016 Offshore Wind Energy Resource Assessment for the United States*. Golden, CO. Available at: <https://www.nrel.gov/docs/fy16osti/66599.pdf>.
- Musial, W. *et al.* (2022) *Offshore Wind Market Report: 2022 Edition*. Available at: <https://www.osti.gov/servlets/purl/1883382/>.
- 610 National Renewable Energy Laboratory (2020) *OpenFAST Documentation Release v2.5.0*. Golden, CO. Available at: <http://openfast.readthedocs.io/en/master/source/user/beamdyn/introduction.html>.
- Principle Power (no date) *WindFloat*. Available at: <https://www.principlepowerinc.com/en/windfloat>.
- Robertson, A., Jonkman, J., Masciola, M., Song, H. (2014) *Definition of the Semisubmersible Floating System for Phase II of OC4*. Golden, CO. Available at: <https://www.nrel.gov/docs/fy14osti/60601.pdf>.
- 615 Sebastian, T. and Lackner, M. (2012) “Analysis of the induction and wake evolution of an offshore floating wind turbine,” *Energies*, 5(4), pp. 968–1000. doi: 10.3390/en5040968.
- Shields, M. *et al.* (2021) “Impacts of turbine and plant upsizing on the levelized cost of energy for offshore wind,” *Applied Energy*. Elsevier Ltd, 298, p. 117189. doi: 10.1016/j.apenergy.2021.117189.
- Siemens Gamesa (2020) *SG 14-222 DD*. Available at: [https://www.siemensgamesa.com/en-int/products-and-](https://www.siemensgamesa.com/en-int/products-and-services/offshore/wind-turbine-sg-14-222-dd)
- 620 [services/offshore/wind-turbine-sg-14-222-dd](https://www.siemensgamesa.com/en-int/products-and-services/offshore/wind-turbine-sg-14-222-dd).
- Sieros, G. *et al.* (2012) “Upscaling wind turbines: theoretical and practical aspects and their impact on the cost of energy,” *Wind Energy*, 15(1), pp. 3–17. doi: 10.1002/we.527.
- Skaare, B. *et al.* (2006) “Integrated dynamic analysis of floating offshore wind turbines,” *European Wind Energy Conference and Exhibition 2006, EWEC 2006*, 3(January), pp. 1834–1842.
- 625 Souza, C. E. S. de and Bachynski-Polić, E. E. (2022) “Design, structural modeling, control, and performance of 20 MW spar floating wind turbines,” *Marine Structures*. Elsevier Ltd, 84(March 2022). doi: 10.1016/j.marstruc.2022.103182.
- Speer, B., Keyser, D. and Tegen, S. (2016) *Floating Offshore Wind in California: Gross Potential for Jobs and Economic Impacts from Two Future Scenarios*. Golden, CO. Available at: <https://www.nrel.gov/docs/fy16osti/65352.pdf>.
- The University of Maine (2021) *Advanced Structures and Composites Center*. Available at:
- 630 <https://composites.umaine.edu/offshorewind/>.
- Thiagarajan, K. P. and Dagher, H. J. (2014) “A Review of Floating Platform Concepts for Offshore Wind Energy Generation,” *Journal of Offshore Mechanics and Arctic Engineering*, 136, pp. 1–6.
- Thresher, R., Robinson, M. and Veers, P. (2008) *Wind Energy Technology: Current Status and R & D Future*. Golden, CO. Available at: <http://www.nrel.gov/docs/fy08osti/43374.pdf>.
- 635 TU Delft (2006) “Chapter 6 Rigid Body Dynamics,” in, pp. 173–176.
- Vestas (2023) *V236-15.0MW*. Available at: <https://us.vestas.com/en-us/products/offshore/V236-15MW>.
- Wang, C. M. *et al.* (2010) “Research on floating wind turbines: A literature survey,” *IES Journal Part A: Civil and Structural Engineering*, 3(4), pp. 267–277. doi: 10.1080/19373260.2010.517395.
- Wu, J. and Kim, M. H. (2021) “Generic upscaling methodology of a floating offshore wind turbine,” *Energies*, 14(24), pp. 1–



640 14. doi: 10.3390/en14248490.

Yao, S. *et al.* (2021) “Aero-structural design and optimization of 50 MW wind turbine with over 250-m blades,” *Wind Engineering*. doi: 10.1177/0309524X211027355.

Yoshimoto, H. *et al.* (2013) “Development of floating offshore substation and wind turbine for Fukushima FORWARD,” in *Proceedings of the International Symposium on Marine and Offshore Renewable Energy*, pp. 1–9.

645